

Effects of *meso*-diarylamino group of porphyrins on optical and electrochemical properties

Tomohiro Higashino^{a,†}, Yamato Fujimori^a, Issei Nishimura^a and Hiroshi Imahori^{*a,b,†}

^aDepartment of Molecular Engineering, Graduate School of Engineering, Kyoto University, Nishikyo-ku, Kyoto 615-8510, Japan

^bInstitute for Integrated Cell-Material Sciences (WPI-iCeMS), Kyoto University, Sakyo-ku, Kyoto 606-8501, Japan

Dedicated to Professor Atsuhiko Osuka on the occasion of his 65th birthday.

Received 10 April 2019

Accepted 14 May 2019

ABSTRACT: Introduction of an electron-donating *meso*-diarylamino group into a porphyrin core affords its broadened and red-shifted absorption and raises the HOMO level of the porphyrin. In this regard, porphyrins with multiple *meso*-diarylamino groups are expected to show unique optical and electrochemical properties depending on the number of the *meso*-diarylamino groups. Herein, we report a series of porphyrins with a different number of the *meso*-diarylamino groups. They were prepared by the iodine(III)-mediated oxidative amination reaction of the corresponding *meso*-free porphyrins. With increasing the number of the *meso*-diarylamino groups, both red shifts and broadening in the absorption and negative shifts in the oxidation potential were observed. Notably, the oxidation potential of the porphyrin with four *meso*-diarylamino groups is comparable to that of tetrathiafulvalene, which is one of representative electron donors, suggesting the potential utility of multiply *meso*-aminated porphyrins as hole-transporting materials and as electron donors forming charge-transfer complexes with electron acceptors. We believe that this study sheds light on porphyrins with multiple electron-donating groups as organic functional materials.

KEYWORDS: porphyrin, amination, electron-donating substituent.

INTRODUCTION

Electron-donating triarylamines and diarylamines have attracted significant interest from chemists because they have been used as important building blocks for organic functional materials in organic light-emitting diodes (OLEDs) [1–5] and organic solar cells (OSCs) [6–11]. In particular, *meso*-aminoporphyrins have drawn increasing attention owing to their great potential as excellent sensitizers for dye-sensitized solar cells (DSSCs) [12–21]. We previously reported the influences of the number and position of *meso*-diarylamino groups on the optical, electrochemical, and photovoltaic properties [22, 23]. Introduction of an electron-donating

meso-diarylamino group into a porphyrin core affords its broadened and red-shifted absorption and raises the HOMO level of the porphyrin. In addition, porphyrins with two *meso*-diarylamino groups display larger broadening and red shifts in the absorption and rise in the HOMO level than porphyrins with one *meso*-diarylamino group. In this regard, porphyrin dyes with multiple *meso*-diarylamino groups are expected to show unique optical and electrochemical properties depending on the number of the *meso*-diarylamino groups. Herein, we report the synthesis and optical and electrochemical properties of porphyrins with multiple *meso*-diarylamino groups N_1P-N_4P in comparison with 5,10,15,20-tetraphenylporphyrin (TPP) as a reference (Fig. 1). We found that both red shifts and broadening in the absorption and negative shifts in the oxidation potential are enhanced with an increase in the number of the *meso*-diarylamino groups.

[†]SPP full member in good standing

*Correspondence to: Hiroshi Imahori, email imahori@scl.kyoto-u.ac.jp.

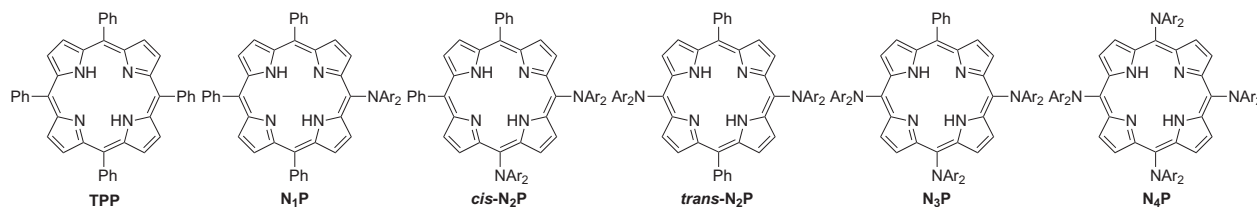


Fig. 1. Molecular structures of *meso*-diarylaminoporphyrins N_1P – N_4P and a reference 5,10,15,20-tetraphenylporphyrin **TPP** (Ar = 4- $CH_3C_6H_4$)

RESULTS AND DISCUSSION

Synthesis and characterization

The synthetic routes of the *meso*-diarylaminoporphyrins N_1P – N_4P are shown in Scheme 1. Previously we found that an iodine(III)-mediated oxidative amination of *meso*-free porphyrin is an effective means to prepare porphyrins with two *meso*-diaryl amino groups [22–25]. Along this line, we aimed to synthesize the *meso*-diarylaminoporphyrins by means of *meso*-free porphyrins **1Zn**–**3Zn** and **4Mg** as key precursors. Zinc *meso*-free porphyrins **1Zn**, *cis*-**2Zn**, and *trans*-**2Zn** were obtained by zinc metalation of the corresponding free-base porphyrins **1H₂**, *cis*-**2H₂**, and *trans*-**2H₂**. Meanwhile, mono-substituted **3Zn** was synthesized by using the corresponding 1,9-bis(*N,N*-dimethylaminomethyl)dipyromethane [26]. The treatment of 5-phenyldipyromethane with *N,N*-dimethylmethyleammonium iodide (Eschenmoser's reagent) [27] and a subsequent reaction with dipyrromethane in the presence of $Zn(OAc)_2$ afforded **3Zn** in 13% yield. Regarding the synthesis of the porphyrin with four *meso*-diaryl amino groups, unsubstituted magnesium(II) porphine **4Mg** was the important intermediate and was prepared according to the literature [28]. In the next step, the iodine(III)-mediated amination reaction of the porphyrins **1Zn**–**3Zn** and **4Mg** with *N,N*-bis(4-methylphenyl)amine provided the corresponding *meso*-diarylaminoporphyrins N_1P – N_4P . Although the yields of N_1P and *cis*- N_2P are moderate (62 and 50%, respectively), those of *trans*- N_2P , N_3P , and N_4P are low (3–20%). The multiple unsubstituted *meso*-positions may induce undesirable side reactions under the oxidative reaction conditions. All the *meso*-diarylaminoporphyrins were fully characterized by high-resolution mass spectrometry and 1H NMR and IR spectroscopies (Figs S1–S6 in supporting information). The structure of the *meso*-tetraaminoporphyrin N_4P has also been supported by its preliminary X-ray crystal analysis (Fig. S7).

Optical properties

The UV-vis absorption spectra of the *meso*-diarylaminoporphyrins N_1P – N_4P and **TPP** in CH_2Cl_2 are depicted in Fig. 2 (see also in Table 1). With increasing the number of the diarylamino groups, the Soret band becomes broadened and blue shifted relative to that

of **TPP**. Notably, a new absorption peak appears at 451–475 nm, which is beneficial to improve the light-harvesting property in the visible region for solar energy conversion. Additionally, the Q bands are also broadened and red shifted compared to **TPP**. Although the molar absorption coefficients (ϵ) of *cis*- N_2P are slightly smaller than those of *trans*- N_2P , the peak positions of *cis*- N_2P and *trans*- N_2P are almost the same.

The steady-state fluorescence spectra of the porphyrins in CH_2Cl_2 are also displayed in Fig. 3. As the number of the diarylamino groups increases, the fluorescence maximum is shifted toward longer wavelengths with reducing the intensity, which agrees with the trend of the absorption properties. The fluorescence lifetimes (τ_f) were measured using the time-correlated single-photon counting (TCSPC) technique (Fig. S8). The τ_f value of the *meso*-aminoporphyrins is decreased gradually with an increase in the number of the *meso*-diaryl amino groups (Table 1). The decreasing tendency is probably attributed to the increased vibrational and rotational degrees of freedom or enhanced charge-transfer (CT) interaction as a result of the introduction of the electron-donating *meso*-diaryl amino groups into the porphyrin core. From the intersection of the normalized absorption and fluorescence spectra, the optical HOMO–LUMO gaps were estimated to be 1.92 eV for **TPP**, 1.81 eV for N_1P , 1.75 eV for *cis*- N_2P and *trans*- N_2P , 1.69 eV for N_3P , and 1.64 eV for N_4P (Table 1). Because *cis*- N_2P and *trans*- N_2P exhibit comparable absorption and fluorescence properties, the position of the *meso*-diaryl amino groups has little impact on the electronic structures of the porphyrins.

Electrochemical properties

The electrochemical properties were studied by cyclic voltammetry (CV) and differential pulse voltammetry (DPV) techniques in CH_2Cl_2 vs. ferrocene/ferrocenium ion (Fc/Fc^+) with tetrabutylammonium hexafluorophosphate (Bu_4NPF_6) as an electrolyte (Fig. S9 and Table 2). All the *meso*-diarylaminoporphyrins N_1P – N_4P exhibit one or two reversible oxidation peaks and two reversible reduction peaks. As the number of the *meso*-diaryl amino groups is increased, the first oxidation potential (E_{ox1}) is significantly shifted to a negative direction. It is noteworthy that the E_{ox1} value of N_4P (–0.08 V) is comparable to that of tetrathiafulvalene

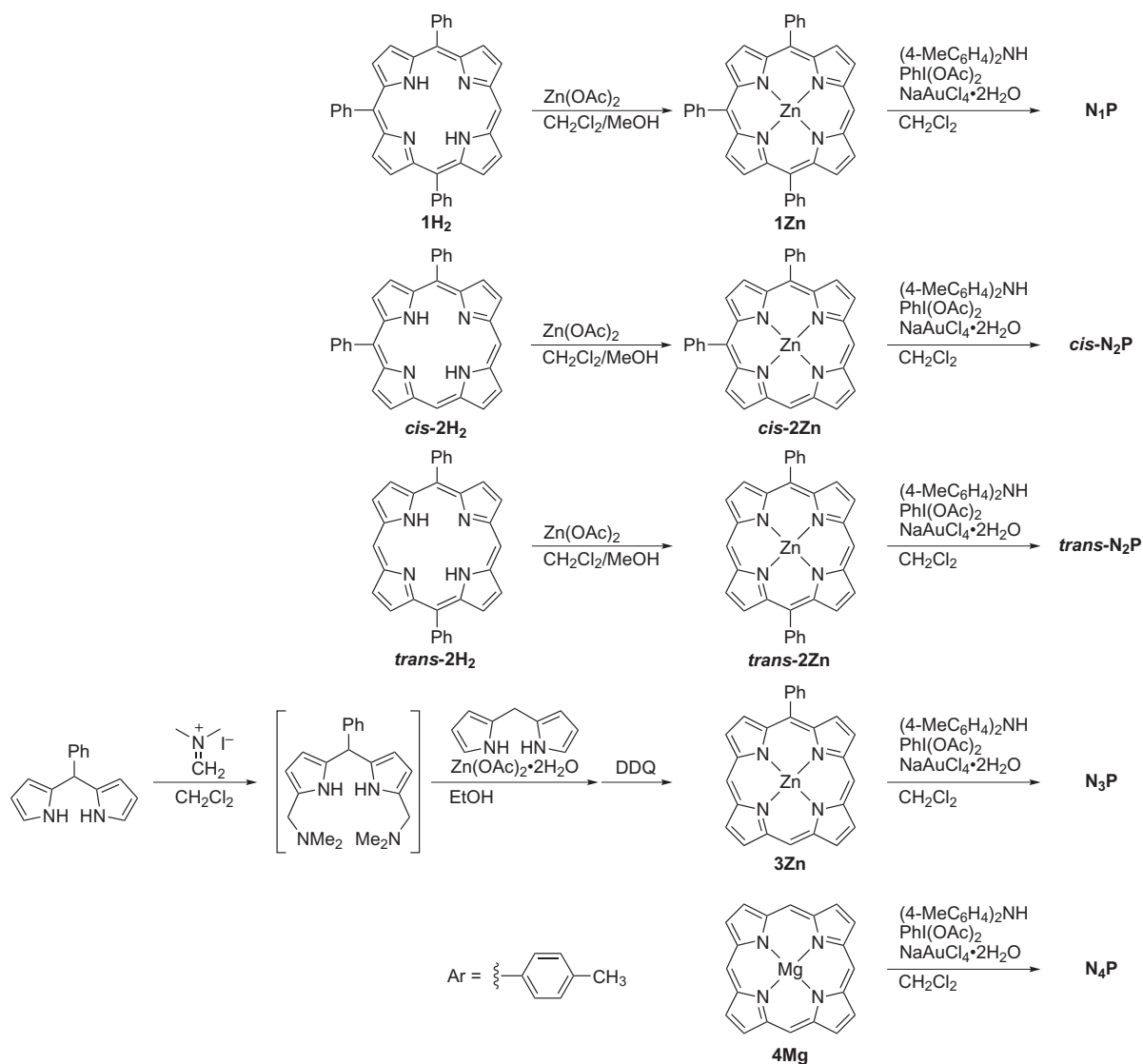
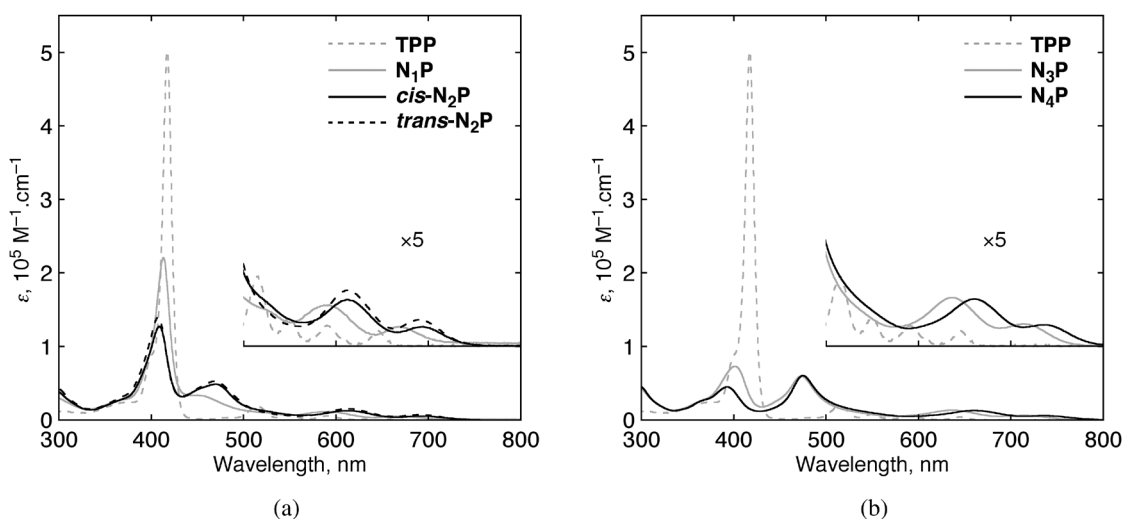
Scheme 1. Synthesis of *meso*-diarylamino porphyrins N_1P – N_4P Fig. 2. UV-vis absorption spectra of (a) TPP, N_1P , $cis-N_2P$, and $trans-N_2P$, and (b) TPP, N_3P , and N_4P in CH_2Cl_2

Table 1. Optical properties of the *meso*-diarylaminoporphyrins in CH₂Cl₂

Porphyrin	λ_{abs} , nm (ϵ , 10 ³ M ⁻¹ · cm ⁻¹)	$\lambda_{\text{em}}^{\text{a}}$, nm	τ_{F} , ns	$E_{\text{opt}}^{\text{b}}$, eV
TPP	418 (500), 516 (19), 550 (7.4), 590 (5.5), 645 (4.1)	650, 715	8.4	1.92
N₁P	413 (220), 451 (33), 592 (11), 668 (5.3)	702	4.8	1.81
<i>cis</i>-N₂P	409 (130), 468 (48), 612 (13), 694 (5.2)	727	4.0	1.75
<i>trans</i>-N₂P	408 (140), 468 (53), 612 (15), 694 (7.2)	727	4.0	1.75
N₃P	402 (73), 474 (60), 638 (13), 713 (6.0)	752	3.3	1.69
N₄P	393 (45), 475 (60), 660 (13), 738 (5.8)	783	2.6	1.64

^aWavelength for emission maximum by exciting at 410 nm. ^bOptical HOMO–LUMO gap.

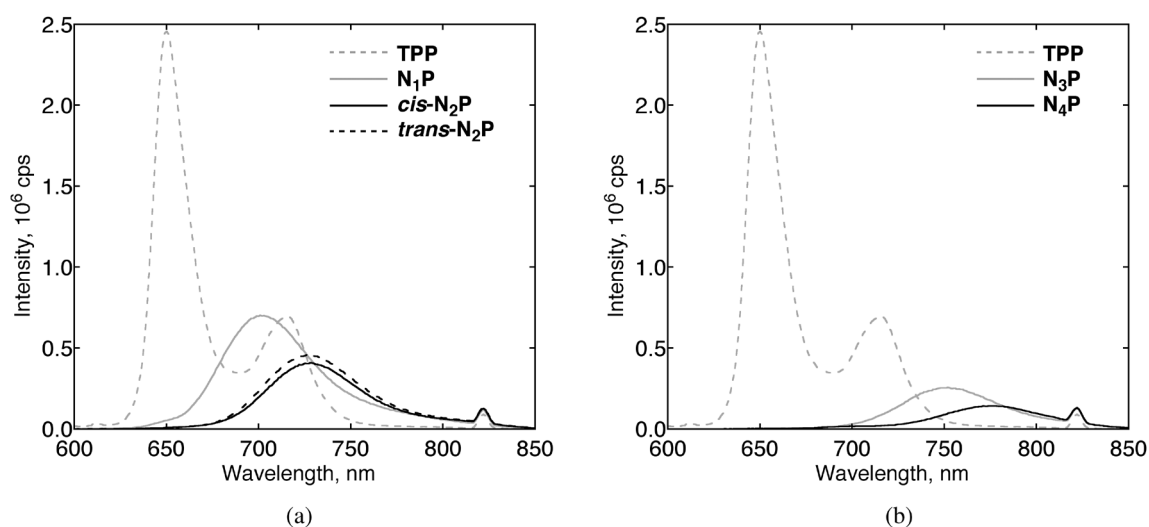


Fig. 3. Fluorescence spectra of (a) **TPP**, **N₁P**, ***cis*-N₂P**, and ***trans*-N₂P**, and (b) **TPP**, **N₃P**, and **N₄P** in CH₂Cl₂. The samples were excited at 410 nm where the absorbances were adjusted to be identical (0.1) for comparison

(TTF) (-0.07 V) [29], which is a typical donor molecule for formation of CT complexes with electron acceptors [30–31]. Thus, the significant electron-rich nature of **N₄P** is highly promising as a hole-transporting material and as an electron donor generating versatile CT complexes. In contrast, the first reduction potential (E_{red1}) is slightly shifted to a positive direction with increasing the number of the *meso*-diaryl amino groups, indicating that *meso*-diaryl amino groups have no significant impact on the porphyrin LUMO levels. When the number of the *meso*-diaryl amino groups is increased, the electrochemical HOMO–LUMO gaps of **N₁P**–**N₄P** become small (Table 2), which is in parallel with the trend for the optical HOMO–LUMO gaps.

Theoretical calculations

To gain further insight into the electronic properties of the *meso*-diarylaminoporphyrins, we performed DFT

Table 2. Electrochemical oxidation and reduction potentials (vs. Fc/Fc^+) of the *meso*-diarylaminoporphyrins in CH₂Cl₂

Porphyrin	E_{ox2} , V	E_{ox1} , V	E_{red1} , V	E_{red2} , V	E_{cv}^{a} , eV
TPP	0.82	0.52	-1.64	-1.93	2.16
N₁P	0.54	0.28	-1.62	-1.95	1.90
<i>cis</i>-N₂P	—	0.23	-1.60	-1.94	1.83
<i>trans</i>-N₂P	—	0.18	-1.59	-1.95	1.77
N₃P	—	0.04	-1.58	-1.94	1.62
N₄P	0.35	-0.08	-1.56	-1.96	1.48

^aElectrochemical HOMO–LUMO gap.

calculations at the B3LYP/6-31G(*d,p*) level. The Kohn–Sham orbitals of **N₁P**–**N₄P** and **TPP** are depicted in Fig. S10. For all the *meso*-diarylaminoporphyrins, the LUMO and LUMO+1 originate from e_{gx} and e_{gy} orbitals

of **TPP**. With increasing the number of the *meso*-diarylamino groups, the energy levels of the LUMO and LUMO+1 are slightly lowered, which largely agrees with the trend for the first and second reduction potentials. Because the LUMO and LUMO+1 possess no orbital distributions on the nitrogen atoms of the *meso*-diarylamino groups, the small negative shifts of the LUMO and LUMO+1 levels can be rationalized by the higher electronegativity of nitrogen atoms than carbon atoms. Meanwhile, as the number of the *meso*-diarylamino groups is increased, the energy level of the HOMO is raised significantly, which is in good agreement with the trend on the first oxidation potentials. The HOMO of **N₁P**–**N₄P** largely stem from the a_{2u} orbital of **TPP** with significant orbital distributions on the *meso*-diarylamino groups. In terms of the introduction of the *meso*-diarylamino groups, the a_{1u} orbital of **TPP** yields HOMO–1 and HOMO–2 of **N₁P**. On the other hand, the a_{1u} orbital gives HOMO–2 of *cis*-**N₂P** and *trans*-**N₂P**, HOMO–3 of **N₃P**, and HOMO–4 of **N₄P**. The HOMO–1 of *cis*-**N₂P** and *trans*-**N₂P**, HOMO–1 and HOMO–2 of **N₃P**, and HOMO–1, HOMO–2, and HOMO–3 of **N₄P** are considerably localized on the *meso*-diarylamino groups. These *meso*-diarylamino-group-based orbitals are responsible for broadening the absorptions. We also performed time-dependent DFT (TD-DFT) calculations at the CAM-B3LYP/6-31G(d) level to evaluate the absorption (Fig. S11 and Table S1). The calculated wavelengths of the lowest-energy Q bands for **N₁P**–**N₄P** (611–653 nm) are red shifted relative to that for **TPP** (597 nm). On the contrary, the calculated wavelengths of the Soret band for **N₁P**–**N₄P** (346–362 nm) exhibit blue shifts in comparison with those for **TPP** (370 nm). Remarkably, for **N₁P**–**N₄P**, calculated new excitations emerge around 430 nm, which can be assigned to the new absorption peaks at 451–475 nm. Moreover, the oscillator strengths of the Q bands for *cis*-**N₂P** ($f = 0.0235$ – 0.0812) are smaller than those for *trans*-**N₂P** ($f = 0.0369$ – 0.0843), which matches with the smaller molar absorption coefficient of *cis*-**N₂P**. Overall, these TD-DFT calculations verify the absorption properties of **N₁P**–**N₄P**.

EXPERIMENTAL

General

Commercially available solvents and reagents were used without further purification unless otherwise mentioned. Triethylamine was distilled from CaH₂. Silica-gel column chromatography and alumina column chromatography were performed with UltraPure Silica Gel (230–400 mesh, SiliCycle) and Alumina, Activated (about 300 mesh, Wako). Thin-layer chromatography (TLC) was performed with Silica gel 60 F₂₅₄ (Merck). ¹H NMR spectra were recorded with a JEOL EX-400

spectrometer (operating at 400 MHz). High-resolution mass spectra (HRMS) were measured on a Thermo Fischer Scientific EXACTIVE spectrometer for ESI measurements. UV-vis absorption spectra were obtained with a Perkin–Elmer Lambda 900 UV-vis/NIR spectrometer. Steady-state fluorescence spectra were recorded by a HORIBA Nanolog spectrofluorometer.

Synthesis

5,10,15-Triphenylporphyrin (**1H₂**) [32], 5,10-diphenylporphyrin (*cis*-**2H₂**) [33], (5,15-diphenylporphyrinato) zinc(II) (*trans*-**2Zn**) [34], and magnesium(II) porphine (**4Mg**) [28] were synthesized according to procedures in the literature.

(5,10,15-Triphenylporphyrinato)zinc(II) (1Zn). To a solution of **1H₂** (46 mg, 0.085 mmol) in CH₂Cl₂ (10 mL) and MeOH (5 mL), Zn(OAc)₂ (78 mg, 0.42 mmol) was added and stirred 5 h. The reaction mixture was concentrated and purified by silica-gel column chromatography (1:1 hexane/CH₂Cl₂) to give **1Zn** (50 mg, 0.083 mmol, 98%) as a purple solid. ¹H NMR (400 MHz, CDCl₃) [35]: δ_H, ppm 10.24 (s, 1H, *meso*-H), 9.39 (d, $J = 4.8$ Hz, 2H, β-H), 9.09 (d, $J = 4.4$ Hz, 2H, β-H), 8.98 (d, $J = 4.0$ Hz, 4H, β-H), 8.23 (m, 6H, Ph), 7.82 (m, 9H, Ph), 7.75 (m, 6H, Ph).

5-[N,N-bis(4-methylphenyl)amino]-10,15,20-triphenylporphyrin (N₁P). To a stirred solution of **1Zn** (40 mg, 0.066 mmol) and bis(4-methylphenyl)amine (66 mg, 0.33 mmol) in CH₂Cl₂ (30 mL), PhI(OAc)₂ (21 mg, 0.066 mmol) and NaAuCl₄·2H₂O (40 mg, 0.10 mmol) were added. After 30 min, the reaction was quenched with aqueous saturated Na₂S₂O₃ and the layers were separated. The organic layer was washed with brine, dried over Na₂SO₄, and concentrated. The crude product was purified by silica-gel column chromatography (2:1 hexane/CH₂Cl₂) and reprecipitation from CH₂Cl₂/MeOH to give **N₁P** (30 mg, 0.041 mmol, 62%) as a green solid. ¹H NMR (CDCl₃, 400MHz): δ_H, ppm 9.22 (d, $J = 4.9$ Hz, 2H, β-H), 8.76 (s, 4H, β-H), 8.71 (d, $J = 4.9$ Hz, 2H, β-H), 8.16 (m, 6H, Ph), 7.78–7.68 (m, 9H, Ph), 7.20 (d, $J = 8.3$ Hz, 4H, Ar-H), 6.97 (d, $J = 8.3$ Hz, 4H, Ar-H), 2.23 (s, 6H, CH₃), -2.45 (s, 2H, NH). HR-MS (ESI): m/z 733.3194 (calcd. for C₅₂H₃₉N₅; [M]⁺⁺ 733.3200). UV-vis (CH₂Cl₂): λ_{max}, nm (log ε) 413 (5.34), 451 (4.52), 592 (4.04), 665 (3.72). Fluorescence (CH₂Cl₂, λ_{ex} = 410 nm): λ_{max}, nm 702. FT-IR (ATR): ν, cm⁻¹ 1502, 1468, 1438, 1346, 1313, 1285, 1256, 1176, 964, 795, 723, 698, 640, 505, 417. Mp > 300 °C.

(5,10-Diphenylporphyrinato)zinc(II) (cis-2Zn). To a solution of *cis*-**2H₂** (62 mg, 0.13 mmol) in CH₂Cl₂ (35 mL) and MeOH (10 mL), Zn(OAc)₂ (123 mg, 0.67 mmol) was added and stirred overnight. The reaction mixture was concentrated and purified by silica-gel column chromatography (1:1 hexane/CH₂Cl₂) to give *cis*-**2Zn** (66 mg, 0.12 mmol, 92%) as a purple solid. ¹H NMR (400 MHz, CDCl₃) [36]: δ_H, ppm 10.24 (s, 2H, *meso*-H), 9.47 (s, 2H, β-H), 9.41 (d, $J = 4.4$ Hz, 2H, β-H), 9.12

(d, $J = 4.4$ Hz, 2H, β -H), 9.02 (s, 2H, β -H), 8.25 (m, 4H, Ph), 7.82–7.75 (m, 6H, Ph).

5,10-Bis[*N,N*-bis(4-methylphenyl)amino]-15,20-diphenylporphyrin (*cis-N₂P*). To a stirred solution of *cis-2Zn* (55 mg, 0.10 mmol) and bis(4-methylphenyl)amine (103 mg, 0.52 mmol) in CH_2Cl_2 (35 mL), $\text{PhI}(\text{OAc})_2$ (34 mg, 0.10 mmol) and $\text{NaAuCl}_4 \cdot 2\text{H}_2\text{O}$ (62 mg, 0.16 mmol) were added. After 30 min, the reaction was quenched with aqueous saturated $\text{Na}_2\text{S}_2\text{O}_3$ and the layers were separated. The organic layer was washed with brine, dried over Na_2SO_4 , and concentrated. The crude product was purified by silica-gel column chromatography (1:1 hexane/ CH_2Cl_2) and reprecipitation from CH_2Cl_2 /hexane to give *cis-N₂P* (43 mg, 0.050 mmol, 50%) as a green solid. $^1\text{H NMR}$ (CDCl_3 , 400 MHz): δ_{H} , ppm 9.12 (d, $J = 4.4$ Hz, 4H, β -H), 9.10 (s, 2H, β -H), 8.67 (s, 2H, β -H), 8.62 (d, $J = 4.4$ Hz, 2H, β -H), 8.09 (m, 4H, Ph), 7.72–7.64 (m, 6H, Ph), 7.17 (d, $J = 8.8$ Hz, 8H, Ar-H), 6.96 (d, $J = 8.8$ Hz, 8H, Ar-H), 2.22 (s, 12H, CH_3), –2.15 (s, 2H, NH). HR-MS (ESI): m/z 852.3929 (calcd. for $\text{C}_{60}\text{H}_{48}\text{N}_6$; $[\text{M}]^+$ 852.3935). UV-vis (CH_2Cl_2): λ_{max} , nm (log ϵ) 409 (5.11), 468 (4.68), 612 (4.11), 694 (3.72). Fluorescence (CH_2Cl_2 , $\lambda_{\text{ex}} = 410$ nm): λ_{max} , nm 727. FT-IR (ATR): ν , cm^{-1} 1501, 1469, 1346, 1313, 1286, 1258, 975, 963, 795, 777, 755, 720, 698, 660, 639, 487, 422. mp $>300^\circ\text{C}$.

5,15-Bis[*N,N*-bis(4-methylphenyl)amino]-10,20-diphenylporphyrin (*trans-N₂P*). To a stirred solution of *trans-2Zn* (40 mg, 0.076 mmol) and bis(4-methylphenyl)amine (75 mg, 0.38 mmol) in CH_2Cl_2 (80 mL), $\text{PhI}(\text{OAc})_2$ (24 mg, 0.076 mmol) and $\text{NaAuCl}_4 \cdot 2\text{H}_2\text{O}$ (45 mg, 0.11 mmol) were added. After 30 min, the reaction was quenched with aqueous saturated $\text{Na}_2\text{S}_2\text{O}_3$ and the layers were separated. The organic layer was washed with brine, dried over Na_2SO_4 , and concentrated. The crude product was purified by silica-gel column chromatography (2:1 hexane/ CH_2Cl_2) and reprecipitation from CH_2Cl_2 /hexane to give *trans-N₂P* (10 mg, 0.012 mmol, 16%) as a green solid. $^1\text{H NMR}$ (CDCl_3 , 400 MHz): δ_{H} , ppm 9.14 (d, $J = 4.9$ Hz, 4H, β -H), 8.63 (d, $J = 4.9$ Hz, 4H, β -H), 8.09 (d, $J = 6.4$ Hz, 4H, Ph), 7.67 (m, 6H, Ph), 7.18 (d, $J = 8.3$ Hz, 8H, Ar-H), 6.97 (d, $J = 8.3$ Hz, 8H, Ar-H), 2.23 (s, 12H, CH_3), –2.13 (s, 2H, NH). HR-MS (ESI): m/z 852.3929 (calcd. for $\text{C}_{60}\text{H}_{48}\text{N}_6$; $[\text{M}]^+$ 852.3935). UV-vis (CH_2Cl_2): λ_{max} , nm (log ϵ) 408 (5.15), 468 (4.72), 612 (4.18), 694 (3.86). Fluorescence (CH_2Cl_2 , $\lambda_{\text{ex}} = 410$ nm): λ_{max} , nm 727. FT-IR (ATR): ν , cm^{-1} 1604, 1503, 1470, 1442, 1345, 1315, 1294, 1258, 1028, 972, 794, 698, 659, 509, 413. mp $>300^\circ\text{C}$.

(5-Phenylporphyrinato)zinc(II) (3Zn). To a stirred solution of 5-phenyldipyrromethane (558 mg, 2.5 mmol) in CH_2Cl_2 (40 mL), *N,N*-dimethylmethyleammonium iodide (975 mg, 5.3 mmol) was added. After 1 h, the reaction mixture was quenched with aqueous NaHCO_3 (100 mL) and the layers were separated. The organic layer was dried over Na_2SO_4 and concentrated. To a stirred solution of the residue and dipyrromethane (367 mg,

2.5 mmol) in ethanol (240 mL), $\text{Zn}(\text{OAc})_2 \cdot 2\text{H}_2\text{O}$ (5.5 g, 25 mmol) was added and refluxed for 2 h. The reaction mixture was cooled to room temperature and DDQ (1.7 g, 7.5 mmol) was added. After 15 min, the reaction was quenched with triethylamine (1.8 mL). After removal of the solvent, the crude product was purified by silica-gel column chromatography (1:1 hexane/ CH_2Cl_2) to give **3Zn** (152 mg, 0.34 mmol, 13%) as a purple solid. $^1\text{H NMR}$ (400 MHz, CDCl_3) [37]: δ_{H} , ppm 10.37 (s, 2H, *meso*-H), 10.32 (s, 1H, *meso*-H), 9.56 (s, 4H, β -H), 9.48 (d, $J = 4.4$ Hz, 2H, β -H), 9.18 (d, $J = 4.4$ Hz, 2H, β -H), 8.27 (m, 2H, Ph), 7.80 (m, 3H, Ph).

5-Phenyl-10,15,20-tris[*N,N*-bis(4-methylphenyl)amino]porphyrin (*N₃P*). To a stirred solution of **3Zn** (130 mg, 0.29 mmol) and bis(4-methylphenyl)amine (570 mg, 2.9 mmol) in CH_2Cl_2 (400 mL), $\text{PhI}(\text{OAc})_2$ (186 mg, 0.58 mmol) and $\text{NaAuCl}_4 \cdot 2\text{H}_2\text{O}$ (345 mg, 0.87 mmol) were added. After 30 min, the reaction was quenched with aqueous saturated $\text{Na}_2\text{S}_2\text{O}_3$ and the layers were separated. The organic layer was washed with brine, dried over Na_2SO_4 , and concentrated. The crude product was purified by silica-gel column chromatography (2:1 hexane/ CH_2Cl_2) and reprecipitation from CH_2Cl_2 /MeOH to give **N₃P** (10 mg, 0.010 mmol, 3%) as a dark green solid. $^1\text{H NMR}$ (CDCl_3 , 400 MHz): δ_{H} , ppm 9.05 (d, $J = 4.8$ Hz, 2H, β -H), 9.01 (q, $J = 4.4$ Hz, 4H, β -H), 8.55 (d, $J = 4.8$ Hz, 2H, β -H), 8.04 (m, 2H, Ph), 7.69–7.62 (m, 3H, Ph), 7.13 (m, 12H, Ar-H), 6.96 (m, 12H, Ar-H), 2.23 (s, 18H, CH_3), –1.86 (s, 2H, NH). HR-MS (ESI): m/z 971.4658 (calcd. for $\text{C}_{68}\text{H}_{57}\text{N}_7$; $[\text{M}]^+$ 971.4670). UV-vis (CH_2Cl_2): λ_{max} , nm (log ϵ) 402 (4.86), 474 (4.78), 638 (4.11), 713 (3.78). Fluorescence (CH_2Cl_2 , $\lambda_{\text{ex}} = 410$ nm): λ_{max} , nm 752. FT-IR (ATR): ν , cm^{-1} 1606, 1502, 1469, 1346, 1314, 1287, 1262, 797, 772, 702, 508, 448. mp $>300^\circ\text{C}$.

5,10,15,20-Tetrakis[*N,N*-bis(4-methylphenyl)amino]porphyrin (*N₄P*). To a stirred solution of **4Mg** (100 mg, 0.30 mmol) and bis(4-methylphenyl)amine (593 mg, 3.0 mmol) in CH_2Cl_2 (100 mL), $\text{PhI}(\text{OAc})_2$ (194 mg, 0.60 mmol) and $\text{NaAuCl}_4 \cdot 2\text{H}_2\text{O}$ (359 mg, 0.90 mmol) were added. After 20 min, the reaction was quenched with aqueous saturated $\text{Na}_2\text{S}_2\text{O}_3$ and the layers were separated. The organic layer was washed with brine, dried over Na_2SO_4 , and concentrated. The crude product was purified by silica-gel column chromatography (2:1 hexane/ CH_2Cl_2) and reprecipitation from CH_2Cl_2 /hexane to give **N₄P** (64 mg, 0.059 mmol, 20%) as a dark brown solid. $^1\text{H NMR}$ (400 MHz, CDCl_3): δ_{H} , ppm 8.93 (s, 8H, β -H), 7.11 (d, $J = 8.8$ Hz, 16H, Ar-H), 6.95 (d, $J = 8.8$ Hz, 16H, Ar-H), 2.22 (s, 24H, CH_3), –1.60 (s, 2H, NH). HR-MS (ESI): m/z 1090.5406 (calcd. for $\text{C}_{76}\text{H}_{66}\text{N}_8$; $[\text{M}]^+$ 1090.5405). UV-vis (CH_2Cl_2): λ_{max} , nm (log ϵ) 393 (4.65), 475 (4.78), 660 (4.11), 738 (3.76). Fluorescence (CH_2Cl_2 , $\lambda_{\text{ex}} = 410$ nm): λ_{max} , nm 783. FT-IR (ATR): ν , cm^{-1} 1606, 1502, 1316, 1287, 1266, 798, 775, 753, 703, 596, 505, 422, 405. mp $>300^\circ\text{C}$.

Electrochemistry

Electrochemical measurements were made using an ALS 660a electrochemical analyzer. Redox potentials were determined by differential pulse voltammetry (DPV) in CH₂Cl₂ containing 0.1 M tetrabutylammonium hexafluorophosphate (Bu₄NPF₆). A glassy carbon (3 mm diameter) working electrode, a Ag/AgNO₃ reference electrode, and a Pt wire counter electrode were employed. Ferrocene was used as an external standard for the DPV measurements.

DFT calculations

All calculations were carried out with the Gaussian 09 program [38]. All structures of porphyrins were fully optimized without any symmetry restraints. The calculations were performed by the DFT method at the restricted B3LYP level of theory with the 6-31G(*d,p*) basis set for C, H, and N. Excitation energies and oscillator strengths for the optimized structures were calculated with the TD-SCF method at the CAM-B3LYP/6-31G(*d*) level.

CONCLUSION

We reported a series of *meso*-diarylaminoporphyrins N₁P–N₄P with different numbers of *meso*-diaryl amino groups. They were synthesized by the iodine(III)-mediated oxidative amination reaction of the corresponding *meso*-free porphyrins. With increasing the number of the *meso*-diaryl amino groups, we found that both red shifts and broadening in the absorption and negative shifts in the oxidation potential are enhanced. Notably, the oxidation potential of the porphyrin with four *meso*-diaryl amino groups is comparable to that of tetrathiafulvalene, which is one of representative electron donors, suggesting the potential utility of multiply *meso*-aminated porphyrins as hole-transporting materials and as electron donors forming charge-transfer complexes with electron acceptors. We believe that this study shed light on porphyrins with multiple electron-donating groups as organic functional materials.

Acknowledgments

This work was supported by the JSPS (KAKENHI Grant Numbers JP18K14198(T.H.) and JP18H03898 (H.I.)).

Supporting information

Figures S1–S11 and Table S1 are given in the supplementary material. This material is available free of charge *via* the Internet at <http://www.worldscinet.com/jpp/jpp.shtml>.

REFERENCES

- Shirota Y and Kageyama H. *Chem. Rev.* 2007; **107**: 953–1010.
- Walzer K, Maennig B, Pfeiffer M and Leo K. *Chem. Rev.* 2007; **107**: 1233–1271.
- Uoyama H, Goushi K, Shizu K, Nomura H and Adachi C. *Nature* 2012; **492**: 234–238.
- Yang Z, Mao Z, Xie Z, Zhang Y, Liu S, Zhao J, Xu J, Chi Z and Aldred MP. *Chem. Soc. Rev.* 2017; **46**: 915–1016.
- Huang T, Jiang W and Duan L. *J. Mater. Chem. C* 2018; **6**: 5577–5596.
- Mishra A, Fischer MKR and Bäuerle P. *Angew. Chem., Int. Ed.* 2009; **48**: 2474–2499.
- Roncali J. *Acc. Chem. Res.* 2009; **42**: 1719–1730.
- Ning Z and Tian H. *Chem. Commun.* 2009: 5483–5495.
- Liang M and Chen J. *Chem. Soc. Rev.* 2013; **42**: 3453–3488.
- Yu Z and Sun L. *Adv. Energy Mater.* 2015; **5**: 1500213.
- Wang J, Liu K, Ma L and Zhan X. *Chem. Rev.* 2016; **116**: 14675–14725.
- Bessho T, Zakeeruddin SM, Yeh C-Y, Diau EW-G and Grätzel M. *Angew. Chem., Int. Ed.* 2010; **49**: 6646–6649.
- Yella A, Lee H-W, Tsao HN, Yi C, Chandiran AK, Nazeeruddin MK, Diau EW-G, Yeh C-Y, Zakeeruddin SM and Grätzel M. *Science* 2011; **334**: 629–634.
- Li L-L and Diau EW-G. *Chem. Soc. Rev.* 2013; **42**: 291–304.
- Urbani M, Grätzel M, Nazeeruddin MK and Torres T. *Chem. Rev.* 2014; **114**: 12330–12396.
- Yella A, Mai C-L, Zakeeruddin SM, Chang S-N, Hsieh C-H, Yeh C-Y and Grätzel M. *Angew. Chem., Int. Ed.* 2014; **53**: 2973–2977.
- Mathew S, Yella A, Gao P, Humphry-Baker R, Curchod BFE, Ashari-Astani N, Tavernelli I, Rothlisberger U, Nazeeruddin MK and Grätzel M. *Nature Chem.* 2014; **6**: 242–247.
- Higashino T and Imahori H. *Dalton Trans.* 2015; **44**: 448–463.
- Kang SH, Jeong MJ, Eom YK, Choi IT, Kwon SM, Yoo Y, Kim J, Kwon J, Park JH and Kim HK. *Adv. Energy Mater.* 2017; **7**: 1602117.
- Song H, Liu Q and Xie Y. *Chem. Commun.* 2018; **54**: 1811–1824.
- Ji J-M, Zhou H and Kim HK. *J. Mater. Chem. A* 2018; **6**: 14518–14545.
- Imahori H, Matsubara Y, Iijima H, Umeyama T, Matano Y, Ito S, Niemi M, Tkachenko NV and Lemmetyinen H. *J. Phys. Chem. C* 2010; **114**: 10656–10665.
- Kurotobi K, Toude Y, Kawamoto K, Fujimori Y, Ito S, Chabera P, Sundström V and Imahori H. *Chem. —Eur. J.* 2013; **19**: 17075–17081.

24. Shen D-M, Liu C, Chen X-G and Chen Q-Y. *J. Org. Chem.* 2009; **74**: 206–211.
25. Higashino T, Kawamoto K, Sugiura K, Fujimori Y, Tsuji Y, Kurotobi K, Ito S and Imahori H. *ACS Appl. Mater. Interfaces* 2016; **8**: 15379–15390.
26. Fan D, Taniguchi M, Yao Z, Dhanalekshmi S and Lindsey JS. *Tetrahedron* 2005; **61**: 10291–10302.
27. Schreiber J, Maag H, Hashimoto N and Eschenmoser A. *Angew. Chem., Int. Ed. Engl.* 1971; **10**: 330–331.
28. Dogutan DK, Ptaszek M and Lindsey JS. *J. Org. Chem.* 2007; **72**: 5008–5011.
29. Adeel S, Abdelhamid ME, Nafady A, Li Q, Martin LL and Bond AM. *RSC Adv.* 2015; **5**: 18384–18390.
30. Ferraris J, Cowan DO, Walatka VJ and Perlstein JH. *J. Am. Chem. Soc.* 1973; **95**: 948–949.
31. Goetz KP, Vermeulen D, Payne ME, Kloc C, McNeil LE and Jurchescu OD. *J. Mater. Chem. C* 2014; **2**: 3065–3076.
32. Plunkett S, Dahms K and Senge MO. *Eur. J. Org. Chem.* 2013: 1566–1579.
33. Hatscher S and Senge MO. *Tetrahedron Lett.* 2003; **44**: 157–160.
34. Maza WA, Vetromile CM, Kim C, Xu X, Zhang XP and Larsen RW. *J. Phys. Chem. A* 2013; **117**: 11308–11315.
35. Tomizaki K, Lysenko AB, Taniguchi M and Lindsey JS. *Tetrahedron* 2004; **60**: 2011–2023.
36. Briñas RP and Brückner C. *Tetrahedron* 2002; **58**: 4375–4381.
37. Mandal AK, Taniguchi M, Diers JR, Niedzwiedzki DM, Kirmaier C, Lindsey JS, Bocian DF and Holten D. *J. Phys. Chem. A* 2016; **120**: 9719–9731.
38. Frisch MJ, Trucks GW, Schlegel HB, Scuseria GE, Robb MA, Cheeseman JR, Scalmani G, Barone V, Mennucci B, Petersson GA, Nakatsuji H, Caricato M, Li X, Hratchian HP, Izmaylov AF, Bloino J, Zheng G, Sonnenberg JL, Hada M, Ehara M, Toyota K, Fukuda R, Hasegawa J, Ishida M, Nakajima T, Honda Y, Kitao O, Nakai H, Vreven T, Montgomery JA Jr, Peralta JE, Ogliaro F, Bearpark M, Heyd JJ, Brothers E, Kudin KN, Staroverov VN, Keith T, Kobayashi R, Normand J, Raghavachari K, Rendell A, Burant JC, Iyengar SS, Tomasi J, Cossi M, Rega N, Millam JM, Klene M, Knox JE, Cross JB, Bakken V, Adamo C, Jaramillo J, Gomperts R, Stratmann RE, Yazyev O, Austin AJ, Cammi R, Pomelli C, Ochterski JW, Martin RL, Morokuma K, Zakrzewski VG, Voth GA, Salvador P, Dannenberg JJ, Dapprich S, Daniels AD, Farkas O, Foresman JB, Ortiz JV, Cioslowski J and Fox DJ. *Gaussian 09*, revision D.01; Gaussian, Inc, Wallingford, CT, 2013.